SUPPORTING INFORMATION

"Closed and semiclosed interhelical structures in membrane vs closed and open structures in detergent for the influenza virus hemagglutinin fusion peptide and correlation of hydrophobic surface area with fusion catalysis" by Ujjayini Ghosh, Li Xie, Lihui Jia, Shuang Liang, and David P. Weliky

1. Reagents. Protected amino acids and resins were obtained from Novabiochem, Sigma-Aldrich, and DuPont, and lipids were obtained from Avanti Polar Lipids. $1\text{-}^{13}C$ Gly and ^{15}N-Phe were obtained from Cambridge Isotopes and then N-Fmoc- or N-t-Boc-protected in our laboratory.[1,2] Other reagents were typically obtained from Sigma-Aldrich.

2. Peptide sequences.

HA3fp20: <u>GLFGAIAGFIENGWEGMIDG</u>GGKKKKG.

HA1fp23: <u>GLFGAIAGFIEGGWTGMIDG</u>WYGGGKKKKG

The underlined residues are N-terminal regions of the HA2 subunit of the hemagglutinin protein of influenza A virus. HA3fp20 and HA1fp23 are chosen because their structures have been extensively characterized in detergent micelles and detergent-rich bicelles. These structures are very different from one another and are predominantly open (HA3fp20) and closed (HA1fp23). The HA3fp20 and HA1fp23 sequences are respectively from the H3 and H1 viral subtypes with sequence variations N12/G12 and E15/T15. Shaded residues 21-23 (WYG) are conserved in both subtypes and are included in HA1fp23 but not HA3fp20. Both peptides have a non-native C-terminal GGKKKKG tag that greatly increases aqueous solubility needed both for peptide purification and for NMR sample preparation.

3. Peptide preparation. HA3fp20 was successfully made with manual Fmoc solid-phase synthesis whereas HA1fp23 could be made with manual t-Boc but not Fmoc synthesis. HF

cleavage after *t*-Boc synthesis was done by Midwest Bio-Tech. Purification was done by reversed-phase HPLC with a C18 column and resulted in >95% peptide purity as estimated from MALDI mass spectra. Peptide concentrations were quantitated with A_{280} and ε=5700 cm^{-1}M^{-1} (HA3fp20) and ε=12660 cm^{-1}M^{-1} (HA1fp23). The typical purified yield was ~10 μmole peptide per 200 μmole resin. Each peptide was either labeled with: G16-^{13}CO, F9-^{15}N; A5-^{13}CO, M17-^{15}N; or G16-^{13}CO, F9 ring-^{2}H (5 sites).

4. **Lipids.** Ether- rather than ester-linked lipids were used because they lack carbonyl (CO) carbons and therefore do not contribute natural abundance (*na*) ^{13}CO signal to the solid-state NMR (SSNMR) spectrum. The lipids were 1,2-di-*O*-tetradecyl-*sn*-glycero-3-phosphocholine (DTPC) and 1,2-di-*O*-tetradecyl-*sn*-glycero-3-[phosphor-*rac*-(1-glycerol)] (DTPG). A DTPC: DTPG (4:1) composition reflects the large fraction of phosphatidylcholine lipid in the membranes of the respiratory epithelial cells infected by influenza virus and the negative charge of these membranes.[3] Membrane binding of the cationic peptide was also enhanced by the negative charge.

5. Vesicle preparation. Lipids were dissolved in chloroform:methanol (9:1) and solvent was removed by nitrogen gas followed by vacuum pumping overnight. The lipid film was suspended in aqueous buffer (10 mM HEPES/5 mM MES/0.01% w/v NaN$_3$) and homogenized with freeze/thaw cycles. Unilamellar vesicles were made by repeated extrusion through a polycarbonate filter with a 100 nm diameter pores.

6. Vesicle fusion assay.[4] "Unlabeled" vesicles were prepared as above. "Labeled" vesicles were similarly prepared and contained an additional 2 mole% fluorescent lipid and 2 mole% quenching lipid, respectively *N*-(7-nitro-2,1,3-benzoxadiazol-4-yl) (ammonium salt) dipalmitoylphosphatidylethanolamine (*N*-NBD-DPPE) and *N*-(lissaminerhodamine B sulfonyl)

(ammonium salt) dipalmitoylphosphatidylethanolamine (N-Rh-DPPE). Labeled and unlabeled vesicles were mixed in 1:9 ratio and the temperature was maintained at 37 $^{\circ}$C. The initial vesicle fluorescence (F_0) was measured, an aliquot of peptide stock was then added, and the time-dependent fluorescence $F(t)$ was subsequently measured in 1 s increments for a total time of 10 min. Peptide-induced fusion between labeled and unlabeled vesicles increased the average fluorophore-quencher distance and resulted in higher fluorescence. An aliquot of Triton X-100 detergent stock was then added and solubilized the vesicles with resultant further increase in the fluorophore-quencher distance and maximal fluorescence, F_{max}. The percent vesicle fusion was calculated as $M(t) = \{[F(t) - F_0] \times 100\}/\{[F_{max} - F_0]\}$. There was typically <2% variation in long-time $M(t)$ among assay replicates. Experimental conditions typically included: (1) initial 1500 μL vesicle suspension with [total lipid] = 150 μM; (2) 467 nm excitation and 530 nm detection wavelengths; (3) 90 μL aliquot of 50 μM peptide stock in water with final [peptide] = 3 μM and peptide:lipid mole ratio = 1:50; (4) 4 s assay dead-time after peptide addition; and (5) 12 μL aliquot of 20% v/v Triton X-100 with final 0.19% v/v Triton X-100.

7. Solid-state NMR sample preparation. Stock peptide solution (0.2 mM) was added dropwise to vesicle suspensions while maintaining the pH at either 5.0 or 7.0. The final peptide:lipid mole ratio =1:25. The suspension was gently vortexed overnight and then ultracentrifuged at 100000g for four hours. The membrane pellet with bound peptide was packed in a 4 mm diameter magic angle spinning (MAS) rotor. There was quantitative binding of the peptide to the membrane as evidenced by $A_{280} < 0.01$ in the supernatant.

8. Solid-state NMR (SSNMR). Spectra were acquired with a 9.4 T Agilent Infinity Plus spectrometer and triple-resonance MAS probe tuned to ^{1}H, ^{13}C, and ^{15}N frequencies or ^{1}H, ^{13}C, and ^{2}H frequencies. The sample rotor was cooled with nitrogen gas at –50 °C and the expected

sample temperature is ~ –30 °C. The REDOR pulse sequence was in time-sequence: (1) a ^{1}H $\pi/2$ pulse; (2) ^{1}H to ^{13}C cross-polarization (CP); (3) dephasing period of variable duration τ; and (4) ^{13}C detection.[5,6] ^{1}H decoupling was applied the dephasing and detection periods. There was interleaved acquisition of the S_0 and S_1 data. The dephasing periods of both acquisitions included a ^{13}C π-pulse at the end of each rotor cycle except the last cycle and the dephasing period of the S_1 acquisition included an additional ^{15}N π-pulse or ^{2}H π-pulse at the midpoint of each cycle. For the S_0 acquisition, there was no net ^{13}C evolution due to ^{13}C-^{15}N or ^{13}C-^{2}H dipolar coupling over a full rotor cycle. For the S_1 acquisition, there was net evolution with consequent reduction in the ^{13}C signal. Typical NMR parameters included 10 kHz MAS frequency, 5.0 µs ^{1}H $\pi/2$-pulse, 50 kHz ^{1}H CP, 60–65 kHz ramped ^{13}C CP, 80 kHz ^{1}H decoupling, and 8.1 µs ^{13}C, 10.0 µs ^{15}N, and 5.0 µs ^{2}H π-pulses with XY-8 phase cycling applied to both pulse trains.[7] Spectra were typically processed using 100 Hz Gaussian line broadening and baseline correction. The $S_0{}^{exp}$ and $S_1{}^{exp}$ intensities were determined from integration of 3 ppm windows centered at the peak ^{13}CO shift. The uncertainties were the RMSD's of spectral noise regions with 3-ppm widths. Spectra were externally referenced to adamantane and assignment of the methylene peak to 40.5 ppm ^{13}C shift allowed direct comparison with liquid-state ^{13}C shifts.[8] Fig. S1 displays the entire shift region of one of the G16/F9 spectra in the absence and presence of baseline correction. In the absence of baseline correction, the typical period of oscillation in the baseline is ~200 ppm which is much larger than the typical full-width-at-half-maximum linewidth of ~5 ppm of a ^{13}CO peak. The ^{13}CO T_1 > 100 s which is typical for organic solids without large-amplitude motions.
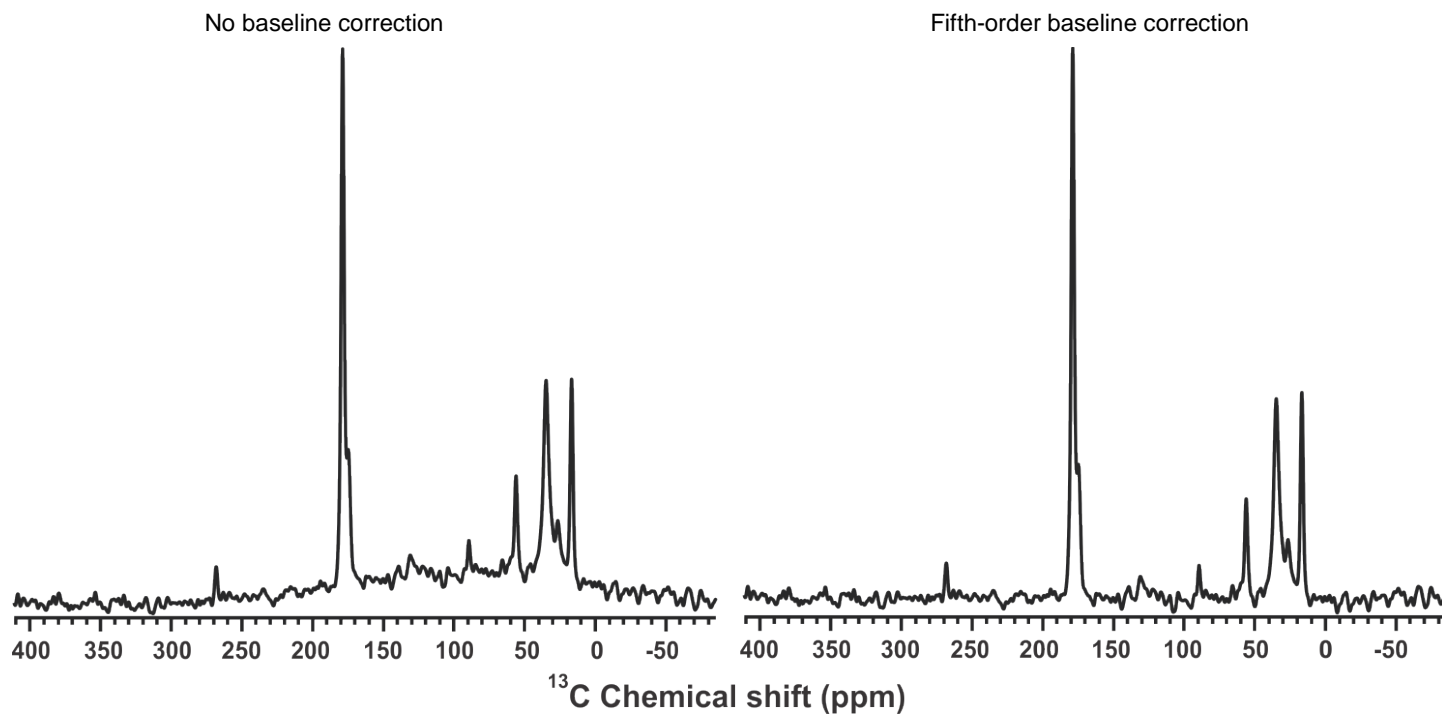
No baseline correction

Fifth-order baseline correction

^{13}C Chemical shift (ppm)

Figure S1. $\tau = 2$ ms S_0 REDOR spectrum of the HA1fp23 pH 7.0 sample (left) without baseline correction and (right) with 5th-order baseline correction.

9. Calculation of $(\Delta S/S_0)^{lab}$. Quantitative analysis of ^{13}CO-^{15}N REDOR includes determination of the $(\Delta S/S_0)^{lab}$ and $(\Delta S/S_0)^{na}$ contributions to $(\Delta S/S_0)^{exp}$ from the labeled (*lab*) and natural abundance (*na*) ^{13}CO nuclei. A $S_0^{lab} = 0.99$ contribution is estimated from the fractional labeling and $S_0^{na} = N \times 0.011$ is estimated for N unlabeled (*unlab*) ^{13}CO sites which contribute to the S_0^{exp} signal. The value of N is not precisely known because the individual spectra of some of the *unlab* sites will not completely overlap with the dominant *lab* spectrum used to set the 3 ppm integration window for S_0^{lab}.[9] We approximate that all the backbone and none of the sidechain ^{13}CO sites contribute to S_0^{exp} so that $N = 26$ for HA3fp20 and $N = 29$ for HA1fp23. The calculated $(\Delta S/S_0)^{lab}$ is typically <10% different than the corresponding $(\Delta S/S_0)^{exp}$ and is not strongly dependent on the precise value of N (Table S2). The derivation of $(\Delta S/S_0)^{lab}$:

$$S_0^{exp} = S_0^{lab} + S_0^{na} = 0.99 + 0.011 \times N \tag{-S1}$$

$$S_1^{exp} = S_1^{lab} + S_1^{na} = S_1^{lab} + \sum_{k=1}^{N} S_{1k} \tag{-S2}$$

For each unlabeled backbone site, $S_0^{na} = 0.011$:

$$\left(\frac{\Delta S}{S_0}\right)^{na} = \left(\frac{S_0^{na} - S_1^{na}}{S_0^{na}}\right) = \frac{0.011 - S_1^{na}}{0.011} \tag{-S3a}$$

$$S_1^{na} = 0.011 - 0.011 \times \left(\frac{\Delta S}{S_0}\right)^{na} \tag{-S3b}$$

Summing over all *unlab* sites:

$$\sum_{k=1}^{N} S_{1k}^{na} = \sum_{k=1}^{N} \left\{0.011 - 0.011 \times \left(\frac{\Delta S}{S_0}\right)_k^{unlab}\right\} = 0.011 \times N - 0.011 \times \sum_{k=1}^{N} \left(\frac{\Delta S}{S_0}\right)_k^{unlab} \tag{-S4}$$

Substituting Eq. S4 into Eq. S2:

$$S_1^{exp} = S_1^{lab} + 0.011 \times N - 0.011 \times \sum_{k=1}^{N} \left(\frac{\Delta S}{S_0}\right)_k^{unlab} \tag{-S5}$$

Combining Eqs. S1, S2, and S5 followed by algebra:

$$\tag{-S6}$$

$$\left(\frac{\Delta S}{S_0}\right)^{exp} = \frac{S_0^{exp} - S_1^{exp}}{S_0^{exp}} = \frac{0.99 - S_1^{lab} + 0.011 \times \sum_{k=1}^{26} \left(\frac{\Delta S}{S_0}\right)_k^{unlab}}{1.276}$$

Rearranging Eq. S6:

$$\left(\frac{\Delta S}{S_0}\right)^{lab} = \frac{0.99 + 0.011 \times N}{0.99} \times \left(\frac{\Delta S}{S_0}\right)^{exp} - 0.011 \times \sum_{k=1}^{N} \left(\frac{\Delta S}{S_0}\right)_k^{unlab}$$

with $\left(\dfrac{\Delta S}{S_0}\right)^{na} = 0.011 \times \sum_{k=1}^{N} \left(\dfrac{\Delta S}{S_0}\right)_k^{unlab}$ -S8

For HA3fp20:

$$\left(\frac{\Delta S}{S_0}\right)^{lab} = 1.2889 \times \left(\frac{\Delta S}{S_0}\right)^{exp} - 0.011 \times \sum_{k=1}^{26} \left(\frac{\Delta S}{S_0}\right)_k^{na}$$ -S9

For HA1fp23:

$$\left(\frac{\Delta S}{S_0}\right)^{lab} = 1.3222 \times \left(\frac{\Delta S}{S_0}\right)^{exp} - 0.011 \times \sum_{k=1}^{29} \left(\frac{\Delta S}{S_0}\right)_k^{na}$$ -S10

Each of the $(\Delta S/S_0)_k^{unlab}$ was calculated using the $^{13}CO_k$ – F9 ^{15}N or the $^{13}CO_k$ – M17 ^{15}N

separation $\equiv r_k$, the corresponding dipolar coupling d_k (Hz) $= \{3066/[r_k(\text{Å})]^3\}$, and the quantum-

Table S1. $(\Delta S/S_0)$ values for the G16 ^{13}CO/F9 ^{15}N samples[a]

τ	HA3fp20					HA1fp23			
(ms)	pH 5.0		pH 7.0			pH 5.0		pH 7.0	
	$(\Delta S/S_0)^{exp}$	$(\Delta S/S_0)^{lab}$	$(\Delta S/S_0)^{exp}$	$(\Delta S/S_0)^{lab}$	$(\Delta S/S_0)^{na}$	$(\Delta S/S_0)^{exp}$	$(\Delta S/S_0)^{lab}$	$(\Delta S/S_0)^{exp}$	$(\Delta S/S_0)^{lab}$
2	0.026(15)	0.032(19)	0.036(23)	0.044(29)	0.002	0.003(29)	0.001(38)	-0.008(28)	-0.012(36)
8	0.079(11)	0.082(15)	0.105(19)	0.115(25)	0.019	0.144(23)	0.167(30)	0.078(33)	0.082(43)
16	0.244(11)	0.278(15)	0.299(21)	0.349(27)	0.037	0.316(17)	0.374(22)	0.338(25)	0.403(32)
24	0.412(8)	0.476(11)	0.495(19)	0.583(24)	0.055	0.494(16)	0.588(21)	0.549(23)	0.659(29)
32	0.511(8)	0.593(11)	0.648(31)	0.769(39)	0.066	0.582(22)	0.691(28)	0.676(23)	0.812(30)
40	0.538(12)	0.616(16)	0.669(30)	0.784(39)	0.078	0.647(15)	0.763(19)	0.759(21)	0.909(28)
48	0.612(13)	0.699(17)	0.723(40)	0.843(52)	0.089	0.687(16)	0.805(21)	0.749(42)	0.884(55)

[a] The calculated $(\Delta S/S_0)^{na}$ are the same for all samples.

Table S2. $(\Delta S/S_0)$ values for the A5 [13]CO/M17 ^{15}N samples[a]

τ (ms)	HA3fp20					HA1fp23			
	pH 5.0		pH 7.0			pH 5.0		pH 7.0	
	$(\Delta S/S_0)^{exp}$	$(\Delta S/S_0)^{lab}$	$(\Delta S/S_0)^{exp}$	$(\Delta S/S_0)^{lab}$	$(\Delta S/S_0)^{na}$	$(\Delta S/S_0)^{exp}$	$(\Delta S/S_0)^{lab}$	$(\Delta S/S_0)^{exp}$	$(\Delta S/S_0)^{lab}$
2	0.014(33)	0.012(43)	0.017(17)	0.016(22)	0.006	–0.014(24)	–0.013(32)	0.015(13)	0.014(17)
8	0.034(26)	0.023(34)	0.041(21)	0.033(27)	0.021	0.059(41)	0.057(55)	0.055(14)	0.052(18)
16	0.074(25)	0.054(32)	0.111(30)	0.102(39)	0.042	0.096(42)	0.085(56)	0.089(30)	0.076(40)
24	0.117(31)	0.084(40)	0.143(22)	0.117(29)	0.068	0.137(36)	0.113(47)	0.136(18)	0.111(24)
32	0.154(27)	0.121(35)	0.229(23)	0.219(29)	0.079	0.198(42)	0.183(56)	0.248(23)	0.249(31)
40	0.244(30)	0.227(39)	0.320(31)	0.327(40)	0.090	0.299(35)	0.305(46)	0.356(12)	0.381(17)
48	0.346(23)	0.351(29)	0.419(20)	0.448(26)	0.098	0.381(30)	0.406(40)	0.456(14)	0.504(18)

[a] The calculated $(\Delta S/S_0)^{na}$ are the same for all samples.

mechanically-derived expression for a pair of coupled spin ½ heteronuclei:

$$(\frac{\Delta S}{S_0})^{sim}\{d,\tau\} = 1 - [J_0(\sqrt{2}\lambda)]^2 + \{2 \times \sum_{k=1}^{5} \frac{[J_k(\sqrt{2}\lambda)]^2}{16k^2 - 1}\}$$

-S11

with $\lambda = d \times \tau$, $\tau \equiv$ duration of the dephasing period, and $J_k \equiv k^{th}$-order Bessel function of the first kind.[10] This is a reasonable approach to r_k estimation because all the $(\Delta S/S_0)^{lab}$ buildups are well-fitted by mixtures of molecules with either closed or semiclosed structure. Tables S1 and S2 list the $(\Delta S/S_0)^{exp}$, $(\Delta S/S_0)^{lab}$, and $(\Delta S/S_0)^{na}$ for the eight data sets.

10. Intermolecular vs Intramolecular G16 [13]CO-F9 ^{15}N proximity. Close intermolecular proximity [G16 [13]CO (molecule 1) to F9 [15]N (molecule 2)] is possible if there are large populations of dimers or higher-order oligomers. This proximity was probed by comparison of the $\Delta S/S_0$ buildups between HA3fp20 samples prepared with either 2 μmole labeled HA3fp20 or 1 μmole labeled and 1 μmole unlabeled HA3fp20 (Fig. S3). Dominant intermolecular proximity would result in $(\Delta S/S_0)^{mixed}/(\Delta S/S_0)^{fully\ lab} < 1$ and dominant intramolecular proximity would result

in $(\Delta S/S_0)^{mixed}/(\Delta S/S_0)^{fully\ lab} \approx 1$. The latter result is observed with much better agreement of

$(\Delta S/S_0)^{mixed}$ with calculated $(\Delta S/S_0)^{intra}$ than with calculated $(\Delta S/S_0)^{inter}$.

Derivation of $(\Delta S/S_0)^{inter}$. Fig. S2 displays an antisymmetric dimer model with the three possible

configurations for a mixture containing p_L fraction labeled peptide and $(1–p_L)$ fraction unlabeled

peptide: (**i**) both labeled with fractional population $p_L{}^2$; (**ii**) one labeled and one unlabeled with

population $[2 \times p_L \times (1–p_L)]$; and (**iii**) both unlabeled with population $(1 – p_L)^2$.
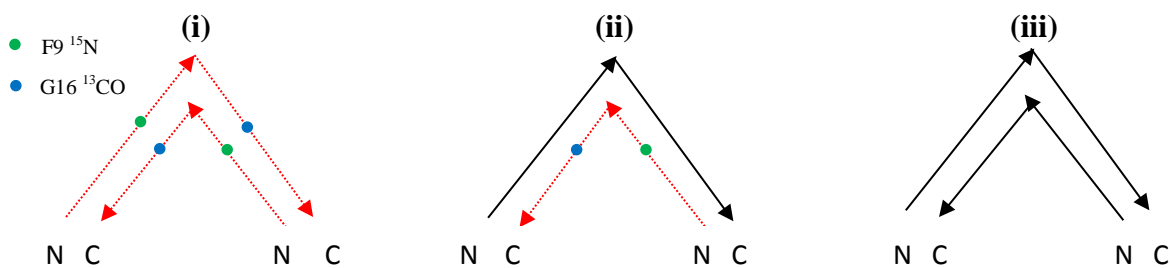

Figure S2. Anti-symmetric dimer configurations of HAfp. Each arrow represents either *N*- or *C*- terminal helices. Labeled HAfp is a red dashed line and unlabeled HAfp is a black line.
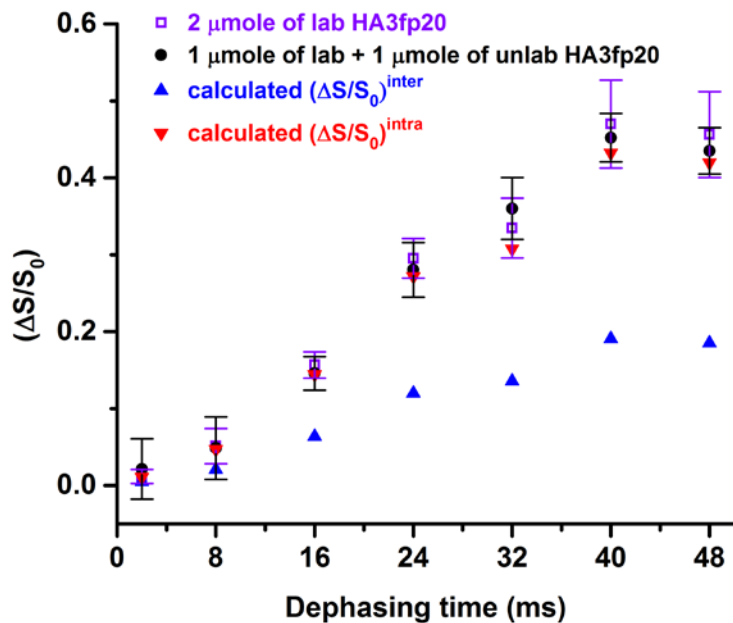

Figure S3. $(\Delta S/S_0)^{exp}$ buildups for pH 5 samples with either 2 μmole G16 ^{13}CO/F9 ^{15}N labeled HA3fp20 or 1 μmole labeled and 1 μmole unlabeled HA3fp20. The calculated $(\Delta S/S_0)^{intra}$ and $(\Delta S/S_0)^{inter}$ for the mixed sample are also displayed.

Table S3. S_0 expressions for intermolecular and intramolecular models [a]

	Intermolecular model			Intramolecular model
	Configuration **i**	Configuration **ii**	Configuration **iii**	
S_0^{lab}	$2p_L^2$	$2p_L \times (1-p_L)$	0	p_L
S_0^{na}	$p_L^2 \times 2N \times 0.011$	$2p_L \times (1-p_L) \times (2N+1) \times 0.011$	$(1-p_L^2) \times 2(N+1) \times 0.011$	$(N+1-p_L) \times 0.011$

[a] $N+1 \equiv$ number of residues in peptide.

The model includes:

1. All labeled molecules contain G16 ^{13}CO and F9 ^{15}N *lab* nuclei. The experimental fractional labeling is 0.99 and the approximation of 1.0 simplifies the calculations.

2. There is G16 ^{13}CO-F9 ^{15}N proximity for both *lab* spin pairs molecules in configuration **i**. Similar results are also obtained for one proximal and one distant *lab* spin pair.

3. There isn't ^{13}CO-^{15}N proximity for *lab* ^{13}CO nuclei in configuration **ii** or *na* ^{13}CO nuclei in all configurations. The consequent approximation $S_1 = S_0$ simplifies the calculations.

Table S3 summarizes the calculated S_0^{lab} and S_0^{na} contributions.

$$S_0^{inter} = S_0^{lab} + S_0^{na} \qquad \text{-S12}$$
$$S_1^{inter} = S_1^{lab} + S_1^{na} \qquad \text{-S13}$$

The only significant contribution to $(\Delta S/S_0)^{inter}$ are from *lab* spin pairs of configuration **i** and are denoted $(\Delta S/S_0)^{lab,i}$. For HA3fp20 with $N+1=27$, algebraic manipulation results in:

$$(\frac{\Delta S}{S_0})^{inter} = \frac{2.00 \, (\frac{\Delta S}{S_0})^{lab,i}}{2.57 \, p_L^2 + 3.17 \, p_L(1-p_L) + 0.59 \, (1-p_L)^2} \qquad \text{-S14}$$

When $p_L = 1.0$:

$$(\frac{\Delta S}{S_0})^{inter}_{p_L=1.0} = 0.778 \times (\frac{\Delta S}{S_0})^{lab,i} \qquad \text{-S15}$$

When $p_L = 0.5$:

$$\left(\frac{\Delta S}{S_0}\right)_{p_L=0.5}^{inter} = 0.316 \times \left(\frac{\Delta S}{S_0}\right)^{lab,i}$$

-S16

The blue up triangles in Fig. S3 are calculated:

$$\left(\frac{\Delta S}{S_0}\right)_{p_L=0.5}^{inter} = 0.316 \times \left(\frac{\Delta S}{S_0}\right)^{lab,i} = \frac{0.316}{0.778} \times \left(\frac{\Delta S}{S_0}\right)_{p_L=1.0}^{lab,i} = 0.406 \times \left(\frac{\Delta S}{S_0}\right)_{p_L=1.0}^{exp}$$

-S17

An alternate dimer structure was also considered in which configuration **i** contains one *lab* pair with close proximity as well as one *lab* pair with distant proximity and $S_1=S_0$:

$$\left(\frac{\Delta S}{S_0}\right)_{p_L=0.5}^{inter} = 0.158 \times \left(\frac{\Delta S}{S_0}\right)^{lab,i} = \frac{0.158}{0.389} \times \left(\frac{\Delta S}{S_0}\right)_{p_L=1.0}^{lab,i} = 0.406 \times \left(\frac{\Delta S}{S_0}\right)_{p_L=1.0}^{exp}$$

-S18

Relative to a dimer structure with both *lab* pairs in close proximity, the $(\Delta S/S_0)$ values are smaller for a structure with one *lab* pair in close proximity. However, the $(p_L=0.5)/(p_L=1.0)$ ratio = 0.41 remains the same for either dimer structure.

<u>Derivation of $(\Delta S/S_0)^{intra}$.</u> The model includes: (1) every labeled peptide contains a *lab* ^{13}CO-^{15}N pair in close intramolecular but not intermolecular proximity; and (2) $S_1^{na}=S_0^{na}$.

$$S_0^{intra} = S_0^{lab} + S_0^{na}$$

-S19

$$S_1^{intra} = S_1^{lab} + S_1^{na}$$

-S20

The expressions from Table S3 and algebraic manipulation with $N+1=27$ result in:

$$\left(\frac{\Delta S}{S_0}\right)^{intra} = \frac{p_L \times \left(\frac{\Delta S}{S_0}\right)^{lab}}{p_L + 0.286}$$

-S21

For $p_L = 1.0$, the result is the same as the intermolecular model:

$$\left(\frac{\Delta S}{S_0}\right)_{p_L=1.0}^{intra} = 0.778 \times \left(\frac{\Delta S}{S_0}\right)^{lab}$$

-S22

For $p_L = 0.5$:

$$\left(\frac{\Delta S}{S_0}\right)^{intra}_{p_L=0.5} = 0.636 \times \left(\frac{\Delta S}{S_0}\right)^{lab} \qquad\qquad\text{-S23}$$

The red down triangles in Fig. S3 are calculated:

$$\left(\frac{\Delta S}{S_0}\right)^{intra}_{p_L=0.5} = 0.636 \times \left(\frac{\Delta S}{S_0}\right)^{lab} = \frac{0.636}{0.778} \times \left(\frac{\Delta S}{S_0}\right)^{lab}_{p_L=1.0} = 0.818 \times \left(\frac{\Delta S}{S_0}\right)^{exp}_{p_L=1.0} \qquad\text{-S24}$$

Eqs.S17 and S24 show that decreasing p_L results in much greater reduction of $(\Delta S/S_0)^{inter}$ than $(\Delta S/S_0)^{intra}$. There is much better agreement of $(\Delta S/S_0)^{exp}{}_{pL=0.5}$ with $(\Delta S/S_0)^{intra}{}_{pL=0.5}$ than with $(\Delta S/S_0)^{inter}{}_{pL=0.5}$ (Fig. S3).

11. Fitting of the ^{13}CO-^{15}N REDOR data with the closed/semiclosed model

The experimentally-derived $(\Delta S/S_0)^{lab}$ buildups fit poorly to a single structure with one dipolar coupling. Fitting is therefore done using models with two or more populations each with different couplings. The **closed/semiclosed model** is based on: (1) a single closed structure with associated distances $r_{cG} \equiv$ G16 ^{13}CO-F9 ^{15}N and $r_{cA} \equiv$ A5 ^{13}CO-M17 ^{15}N and corresponding dipolar couplings d_{cG} and d_{cA}; and (2) a single semiclosed structure with distances r_{sG} and r_{sA} and couplings d_{sG} and d_{sA}. Each sample type (HA3fp20 vs HA1fp23 and pH 5 vs pH 7) is a mixture of a closed and semiclosed peptides with respective fractions f_c and $f_s = 1 - f_c$. The f_{c1}, f_{c2}, f_{c3}, and f_{c4} respectively correspond to the HA3fp20/pH 5, HA3fp20/pH 7, HA1fp23/pH 5, and HA1fp23/pH 7 samples. The χ^2 are calculated for an array of $d_{cG}, d_{cA}, d_{sG}, d_{sA}, f_{c1}, f_{c2}, f_{c3}$, and f_{c4} values with the $(\Delta S/S_0)^{sim}$ for each d calculated by Eq. S11:

$$\chi^2(f_{c1}, f_{c2}, f_{c3}, f_{c4}, d_{cG}, d_{sG}, d_{sA}, d_{sG})$$

$$= \sum_{i=1}^{7} \frac{[(\frac{\Delta S}{S_0})_i^{lab} - \{f_{c1} \times (\frac{\Delta S}{S_0})_i^{sim}(d_{cG})\} - (1-f_{c1}) \times (\frac{\Delta S}{S_0})_i^{sim}(d_{sG})]^2}{(\sigma_i^{lab})^2} + \sum_{j=1}^{7} \frac{[(\frac{\Delta S}{S_0})_j^{lab} - \{f_{c2} \times (\frac{\Delta S}{S_0})_j^{sim}(d_{cG})\} - (1-f_{c2}) \times (\frac{\Delta S}{S_0})_j^{sim}(d_{sG})]^2}{(\sigma_j^{lab})^2}$$

$$+ \sum_{k=1}^{7} \frac{[(\frac{\Delta S}{S_0})_k^{lab} - \{f_{c3} \times (\frac{\Delta S}{S_0})_k^{sim}(d_{cG})\} - (1-f_{c3}) \times (\frac{\Delta S}{S_0})_k^{sim}(d_{sG})]^2}{(\sigma_k^{lab})^2} + \sum_{l=1}^{7} \frac{[(\frac{\Delta S}{S_0})_l^{lab} - \{f_{c4} \times (\frac{\Delta S}{S_0})_l^{sim}(d_{cG})\} - (1-f_{c4}) \times (\frac{\Delta S}{S_0})_l^{sim}(d_{sG})]^2}{(\sigma_l^{lab})^2}$$

$$+ \sum_{m=1}^{7} \frac{[(\frac{\Delta S}{S_0})_m^{lab} - \{f_{c1} \times (\frac{\Delta S}{S_0})_m^{sim}(d_{cA})\} - (1-f_{c1}) \times (\frac{\Delta S}{S_0})_m^{sim}(d_{sA})]^2}{(\sigma_m^{lab})^2} + \sum_{n=1}^{7} \frac{[(\frac{\Delta S}{S_0})_n^{lab} - \{f_{c2} \times (\frac{\Delta S}{S_0})_n^{sim}(d_{cA})\} - (1-f_{c2}) \times (\frac{\Delta S}{S_0})_n^{sim}(d_{sA})]^2}{(\sigma_n^{lab})^2}$$

$$+ \sum_{p=1}^{7} \frac{[(\frac{\Delta S}{S_0})_p^{lab} - \{f_{c3} \times (\frac{\Delta S}{S_0})_p^{sim}(d_{cA})\} - (1-f_{c3}) \times (\frac{\Delta S}{S_0})_p^{sim}(d_{sA})]^2}{(\sigma_p^{lab})^2} + \sum_{q=1}^{7} \frac{[(\frac{\Delta S}{S_0})_q^{lab} - \{f_{c4} \times (\frac{\Delta S}{S_0})_q^{sim}(d_{cA})\} - (1-f_{c4}) \times (\frac{\Delta S}{S_0})_q^{sim}(d_{sA})]^2}{(\sigma_q^{lab})^2}$$

-S25

Table S4. Best-fit parameters of the closed/semiclosed model [a,b]

HA3fp20 pH 5.0 f_{c1}	HA3fp20 pH 7.0 f_{c2}	HA1fp23 pH 5.0 f_{c3}	HA1fp23 pH 7.0 f_{c4}	d_{cG} - Hz	d_{cA} - Hz	d_{sG} - Hz	d_{sA} - Hz	r_{cG} - Å	r_{cA} - Å	r_{sG} - Å	r_{sA} - Å
0.35(2)	0.55(4)	0.53(3)	0.68(3)	52.1(1.2)	19.5(5)	19.7(6)	5.5(8)	3.89(3)	5.40(5)	5.38(5)	8.25(40)

[a] Fitting is done with the f_c's ≡ fractional populations of closed structure and d's ≡ dipolar couplings. The corresponding best-fit r's are calculated from the best-fit d's using $r(\text{Å}) = [3066/d(\text{Hz})]^{1/3}$ which reflects a coupling that isn't motionally-averaged.

[b] The fitting is statistically reasonable because $\chi^2_{min} = 50$ is comparable to the number of degrees of fitting = 48. The uncertainty of a best-fit parameter value in parentheses is based on the difference between parameter values for $\chi^2_{min} + 3$ vs χ^2_{min}.

Table S5. $(\Delta S/S_0)$ values for $d = 51.7$ Hz [a]

τ (ms)	$(\Delta S/S_0)$ Eq. S11	$(\Delta S/S_0)$ SIMPSON
2	0.011	0.014
8	0.171	0.179
16	0.562	0.570
24	0.913	0.918
32	1.043	1.046
40	0.972	0.978
48	0.866	0.876

[a] This d corresponds to $r = 3.90$ Å.

[b] The SIMPSON calculation is based on the experimental pulse sequence with input parameters that include the MAS frequency, ^{13}C and ^{15}N pulse fields and durations, and ^{13}CO chemical shift offset and anisotropy.

Each summation is for one buildup with seven dephasing times. The σ^{lab} is the $(\Delta S/S_0)^{lab}$ uncertainty and is calculated using the RMSD spectral noise.[6] The best-fit corresponds to minimum $\chi^2 \equiv \chi^2_{min}$. Table S4 lists the best-fit parameters including uncertainties and χ^2_{min}. The calculated $(\Delta S/S_0)$ values using the analytical expression of Eq. 11 are typically within 0.01 of the values calculated using the SIMPSON program which incorporates the experimental MAS frequency, pulse fields and durations, and chemical shift offsets and anisotropies. Table S5 displays calculated $(\Delta S/S_0)$ from both approaches for $d = 51.7$ Hz which corresponds to $r = 3.90$ Å.

12. Alternative fitting models

Fitting was done using alternative models but none of these fittings resulted in χ^2 values as statistically reasonable as the closed/semiclosed model. These fittings are done with the G16/F9 $(\Delta S/S_0)$ buildups because they are significantly larger than the A5/M17 buildups. Fitting is first done with the closed/semiclosed model for the two HA3fp20 buildups and separately for the two HA1fp23 buildups.

The **closed/open model** is based on a single closed structure with r_{cG} and d_{cG} and an open structure which does not contribute to $(\Delta S/S_0)$ because r_{oG} is large and $d_{oG} \approx 0$. The four buildups are fitted simultaneously to the f_c and d_{cG} parameters:

$$\chi^2(f_{c1},f_{c2},f_{c3},f_{c4},d_{cG}) = \sum_{i=1}^{7} \frac{[(\frac{\Delta S}{S_0})_i^{lab} - \{f_{c1} \times (\frac{\Delta S}{S_0})_i^{sim}(d_{cG})\}]^2}{(\sigma_i^{lab})^2} + \sum_{j=1}^{7} \frac{[(\frac{\Delta S}{S_0})_j^{lab} - \{f_{c2} \times (\frac{\Delta S}{S_0})_j^{sim}(d_{cG})\}]^2}{(\sigma_j^{lab})^2}$$
$$+ \sum_{k=1}^{7} \frac{[(\frac{\Delta S}{S_0})_k^{lab} - \{f_{c3} \times (\frac{\Delta S}{S_0})_k^{sim}(d_{cG})\}]^2}{(\sigma_k^{lab})^2} + \sum_{l=1}^{7} \frac{[(\frac{\Delta S}{S_0})_l^{lab} - \{f_{c4} \times (\frac{\Delta S}{S_0})_l^{sim}(d_{cG})\}]^2}{(\sigma_l^{lab})^2} \qquad \text{-S26}$$

The **closed/semiclosed/open model** is based on earlier studies interpreted to support ~0.2 fraction of open structure at low pH.[11,12] The two pH 5 buildups are fitted with a 0.2 fraction open structure:

$$\chi^2\{f_{c1}, f_{c3}, d_{cG}, d_{sG}\} = \sum_{i=1}^{7} \frac{[(\frac{\Delta S}{S_0})_i^{lab} - f_{c1} \times (\frac{\Delta S}{S_0})_i^{sim}\{d_{cG}\} - (0.8 - f_{c1}) \times (\frac{\Delta S}{S_0})_i^{sim}\{d_{sG}\} - 0.2 \times (\frac{\Delta S}{S_0})_i^{sim}\{d_{oG}\}]}{(\sigma_i^{lab})^2}$$

$$+ \sum_{k=1}^{7} \frac{[(\frac{\Delta S}{S_0})_k^{lab} - f_{c3} \times (\frac{\Delta S}{S_0})_k^{sim}\{d_{cG}\} - (0.8 - f_{c3}) \times (\frac{\Delta S}{S_0})_k^{sim}\{d_{sG}\} - 0.2 \times (\frac{\Delta S}{S_0})_k^{sim}\{d_{oG}\}]}{(\sigma_k^{lab})^2}$$ -S27

Fitting is done with $r_{oG} = 11.5$ Å and with $r_{oG} = 7.2$ Å which are respectively for the open structure of HA3fp20 in detergent and membranes. The membrane structure is the N-helix from residues 1-10, C-helix from residues 13-20, and turn determined using the ^{13}C shifts of a minor set of E11 inter-residue crosspeaks.[11] Fitting is done for an array of either d_{cG}, d_{sG}, and f_c values or only f_c values with fixed d_{cG}, d_{sG}, and d_{oG} derived from structures of HAfp in detergent and membranes.

Table S6 lists the best-fit parameters of the different models and Figs. S4-S6 display plots of experimental and best-fit $(\Delta S)/S_0$.

Table S6. Best-fit parameters of the models used to fit the G16/F9 SSNMR REDOR data[a,b]

Model	HA3fp20 pH 5.0 f_{c1}	HA3fp20 pH 7.0 f_{c2}	HA1fp23 pH 5.0 f_{c3}	HA1fp23 pH 7.0 f_{c4}	d_{cG} - Hz (r_{cG} - Å)	d_{sG} - Hz (r_{cG} -Å)	χ^2_{min}	deg. of freedom ν_f
Closed/semiclosed								
Simultaneous fit	0.36	0.55	0.53	0.68	52.1 (3.89)	19.2 (5.42)	34	22
HA3fp20 fit	0.33	0.53			56.8 (3.78)	20.2 (5.33)	15	10
HA1fp23 fit			0.51	0.66	55.0 (3.82)	20.7 (5.29)	19	10
Closed/open	0.60	0.78	0.71	0.90	47.9 (4.00)		142	23
Closed/semiclosed/open								
$d_{oG}(r_{oG}) = 2.0$ Hz (11.5 Å)	0.58		0.68		43.2 (4.14)	18.1 (5.14)	92	10
$d_{oG}(r_{oG}) = 8.2$ Hz (7.2 Å)	0.51		0.61		41.4 (4.20)	21.8 (5.20)	77	10
$d_{cG}(r_{cG}) = 51.7$ Hz (3.9 Å) $d_{sG}(r_{sG}) = 18.4$ Hz (5.5 Å) $d_{oG}(r_{oG}) = 2.0$ Hz (11.5 Å)	0.47		0.62				137	12
$d_{cG}(r_{cG}) = 51.7$ Hz (3.9 Å) $d_{sG}(r_{sG}) = 18.4$ Hz (5.5 Å) $d_{oG}(r_{oG}) = 8.2$ Hz (7.2 Å)	0.44		0.60				83	12

[a] Fitting parameters include $d_G(r_G) \equiv$ dipolar coupling (G16 ^{13}CO-F9 ^{15}N distance) and $f \equiv$ mole fraction.
[b] The typical χ^2_{min}+2-based parameter uncertainties for the closed/semiclosed model are: f, 0.03; and $d_G(r_G)$, 1 Hz (0.02 Å).
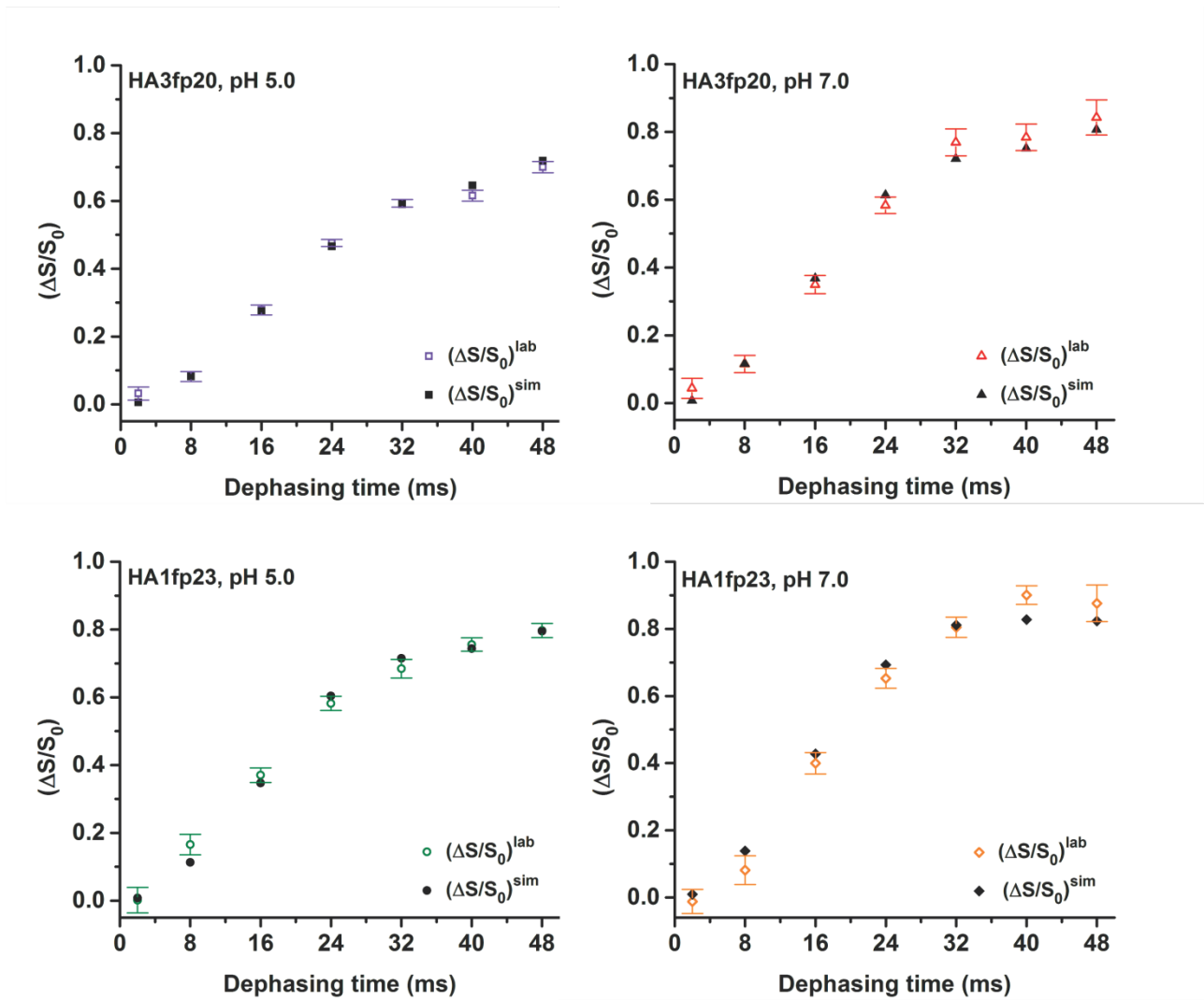
Figure S4. Plots of experimental G16/F9 and best-fit ($\Delta S/S_0$) from the closed/semiclosed model. The HA3fp20 (top) and HA1fp23 (bottom) data are fitted separately.
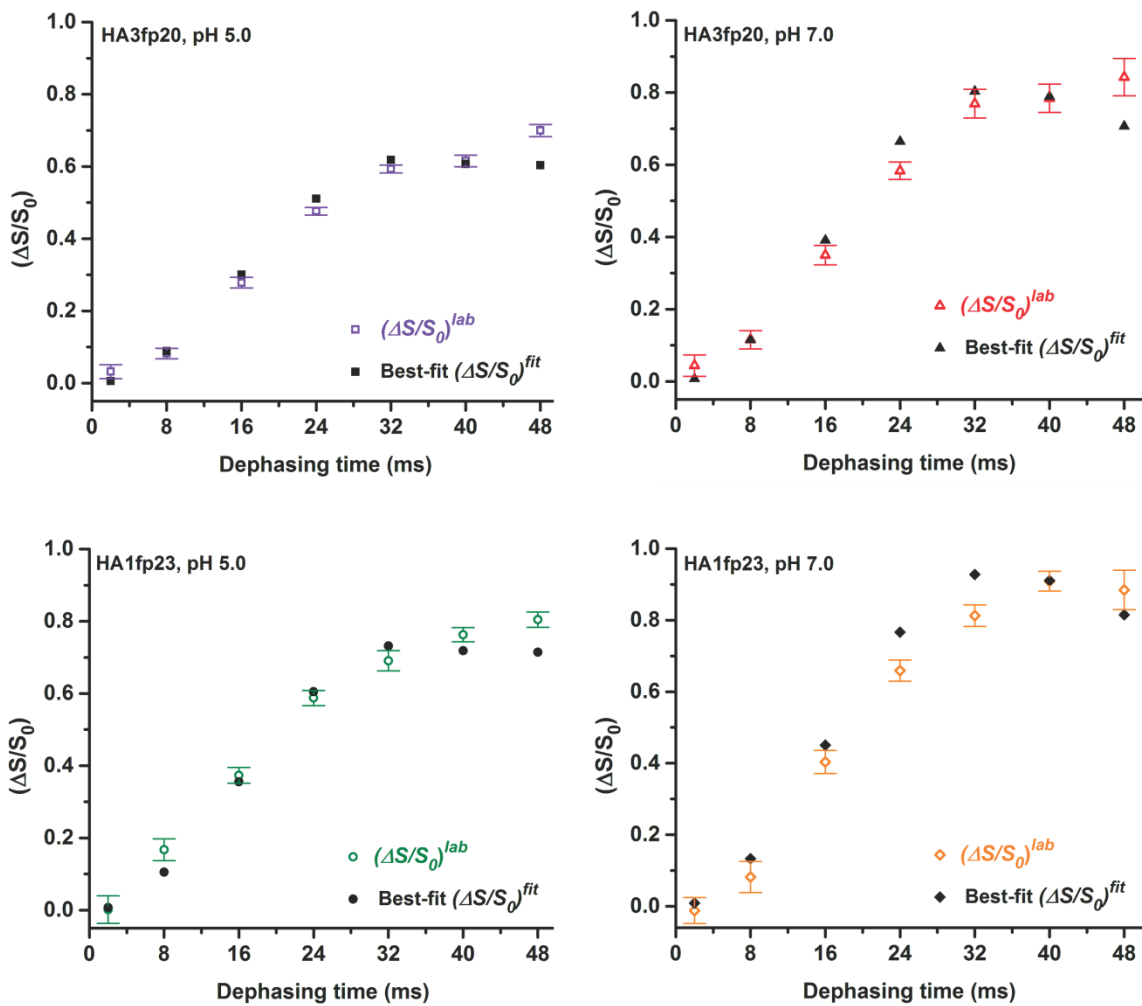
Figure S5. Plots of experimentally-derived G16/F9 $(\Delta S/S_0)^{lab}$ and best-fit $(\Delta S/S_0)$ from the closed/open model.
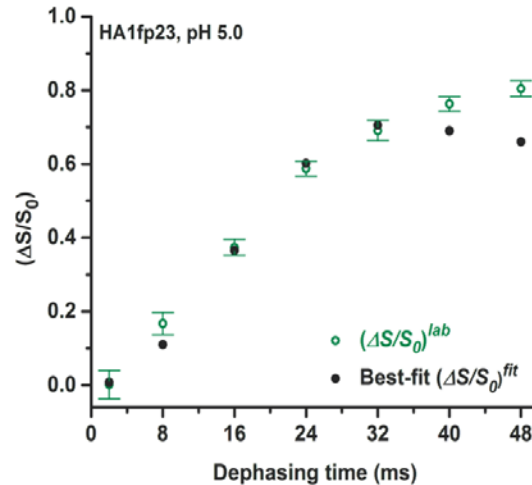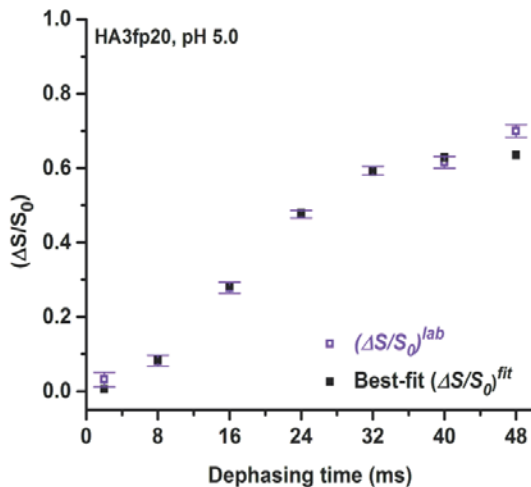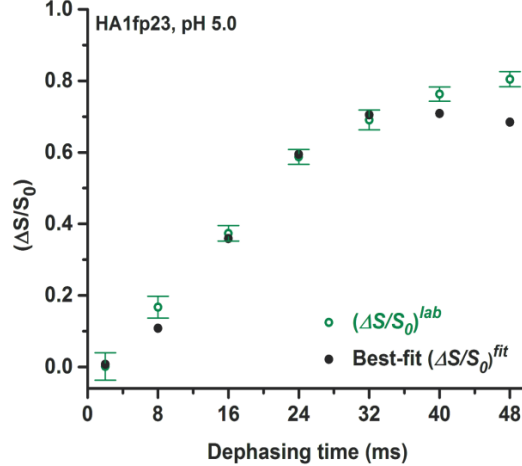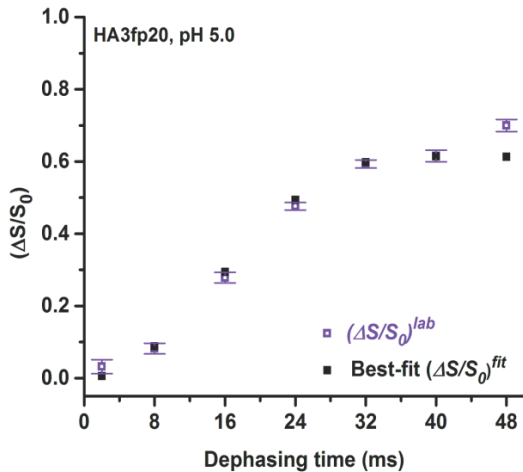
Figure S6. Plots of experimentally-derived G16/F9 $(\Delta S/S_0)^{lab}$ and best-fit $(\Delta S/S_0)$ from the closed/semiclosed/open model using (top) d_{oG} (r_{oG}) = 2.0 Hz (11.5 Å) and (bottom) d_{oG} (r_{oG}) = 8.2 Hz (7.2 Å). The d_{cG} and d_{sG} are fixed.

The fittings yield $r_{cG} \approx 3.9$ Å and $r_{sG} \approx 5.4$ Å that are consistent with earlier structures in detergent and membranes. Because $(\Delta S/S_0)^{open} \approx 0$, the models that include open structure result in a greater fraction closed structure relative to the closed/semiclosed model. The lowest χ^2_{min} is obtained for the closed/semiclosed model and this model is also statistically reasonable based on χ^2_{min} close to ν_f. Much higher χ^2_{min}'s are obtained for the other models that include open structure and the $\chi^2_{min} \gg \nu_f$. The closed/semiclosed model is therefore considered most likely.

Very similar best-fit parameters are obtained for simultaneous fitting of all buildups and for separate fittings of the HA3fp20 and HA1fp23 buildups. This supports the hypothesis of a single closed structure and a single semiclosed structure common to both peptides.
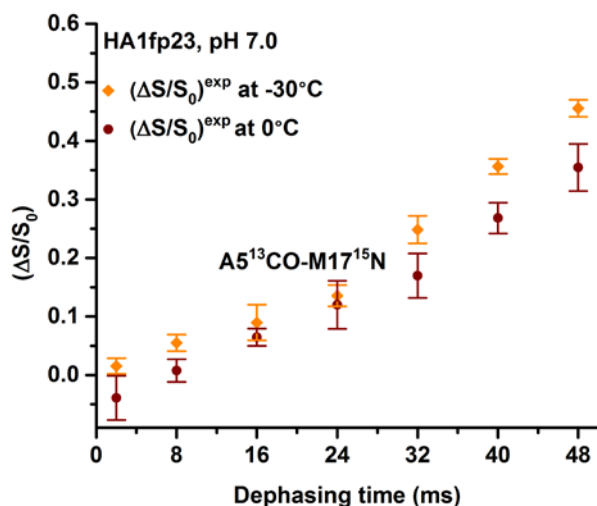
13. Buildups at different temperatures

Figure S7. ^{13}CO-^{15}N $(\Delta S/S_0)^{exp}$ buildups with sample temperatures of ~ –30 and ~ 0 $^{\circ}$C (cooling gas temperatures of –50 and – 20 $^{\circ}$C, respectively). The signal-per ^{13}C nucleus-per scan at 0 $^{\circ}$C is about half that at –30 $^{\circ}$C.

13. ^{13}CO-^{2}H fitting.

Fig. S8 displays fitting of the $(\Delta S/S_0)^{exp}$ buildup of HA3fp20 at pH 5 with G16 ^{13}CO and F9 ring ^{2}H labeling. The fitting model is: (1) closed and semiclosed structures with $f_c = 0.35$ and $f_s = 0.65$ (Table S4); (2) ^{13}CO-^{2}H $d_{cD} \approx 0$ that reflects $r_{CD} > 8$ Å in the closed structure because the F9 ring points away from the C-helix; and (3) fitting parameter d_{sD} that reflects ^{13}CO-^{2}H proximity in the semiclosed structure because of the F9 ring location in the interhelical space. The buildup of $(\Delta S/S_0)^{exp}$ is fitted to $[0.65 \times (\Delta S/S_0)^{sim}]$ where the $(\Delta S/S_0)^{sim}$ are for isolated ^{13}CO-^{2}H spin pairs with a single value of d_{sD} and the $(\Delta S/S_0)^{sim}$ are calculated using the SIMPSON program which incorporates the 10 kHz MAS frequency, ^{13}C and ^{2}H pulse fields and durations, and ^{13}CO and ^{2}H anisotropies. The best-fit $d_{sD} = 19(1)$ Hz corresponds to $r_{sD} = 6.2(1)$ Å. The fitting model is semi-quantitative because of uncertainties which include: (1)
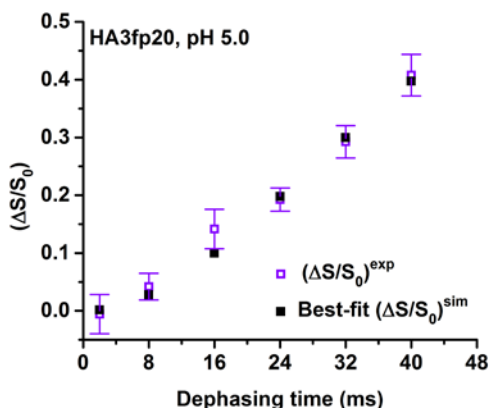
G16 ^{13}CO-F9 ring ^{2}H REDOR

Figure S8. ^{13}CO-^{2}H $(\Delta S/S_0)^{exp}$ and best-fit $[0.65 \times (\Delta S/S_0)^{sim}]$ buildups with $d_{sD} = 19$ Hz. The HA3fp20 sample at pH 5 contained G16 ^{13}CO and F9 ring ^{2}H labeling.

five ring ^{2}H's so that the $(\Delta S/S_0)^{exp}$ reflect five somewhat different r_{sD}'s as well as a small contribution from the five different r_{cD}'s; (2) the calculated $r_{SD} = 6.2$ Å is based on rigid ^{13}CO-^{2}H spin pairs but would be smaller if there were motional averaging of ^{13}CO-^{2}H dipolar coupling from rotation of the F9 ring; and (3) fitting with $(\Delta S/S_0)^{lab}$ rather than $(\Delta S/S_0)^{exp}$ would likely lead to ~20% larger best-fit d_{SD} and ~5% smaller r_{sD} (Table S2).

14. Structural models. The structural pictures are generated using the PYMOL and MOLMOL programs. Table S7 lists the backbone dihedral angles of the closed, semiclosed, and open structural models. NMR data in detergent are the basis for the closed (HA1fp23 at pH 7.4) and open (HA3fp20 at pH 5.0) structures.[13,14] The semiclosed structure is based on SSNMR data of the present and earlier papers for HA3fp20 and HA1fp23 in membranes at pH 5 and 7.[11] The *N*-helix/turn/*C*-helix geometry is similar to the closed structure and the closed structure dihedral angles are used for residues 1-10 and 13-22. The semiclosed residue 11 and 12 angles are based on TALOS analysis of ^{13}C shifts. The semiclosed structure was energy-minimized using the YASARA program.[15] The initial structure was the above backbone with sidechain positions from a MD simulation structure with protonated E11 (F1 structure).[16] The semiclosed backbone was stable under energy minimization and there were small changes in sidechain positions.
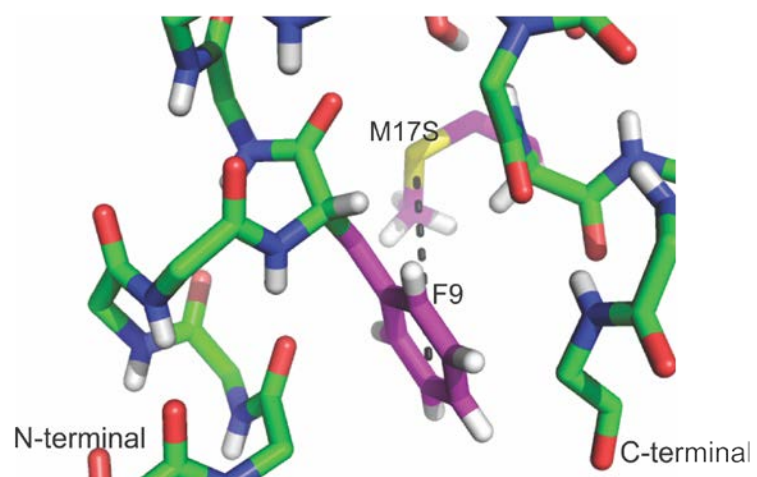
Figure S9. View of the M17 S-F9 ring hydrophobic interaction in the energy-minimized HA3fp20 structure.

Table S7: Backbone dihedral angles of the HAfp structures.

Residue	Closed/Semiclosed		Open	
	φ	ψ	φ	ψ
G1		-107.8 (97.2)		-160.1 (0.3)
L2	-64.6 (2.3)	-50.6 (2.6)	-46.7 (1.1)	-43.7 (0.1)
F3	-64.2 (0.9)	-46.5 (1.6)	-51.9 (1.6)	-34.9 (0.5)
G4	-56.9 (1.0)	-32.8 (0.8)	-67.6 (0.6)	-34.7 (2.5)
A5	-68.8 (1.3)	-46.4 (0.9)	-72.3 (2.2)	-36.4 (2.6)
I6	-60.9 (0.9)	-52.1 (0.8)	-57.9 (1.1)	-40.6 (1.1)
A7	-65.9 (0.8)	-42.2 (0.4)	-65.6 (1.3)	-35.1 (4.6)
G8	-63.3 (0.5)	-34.8 (0.8)	-53.5 (5.1)	-52.1 (5.7)
F9	-64.8 (0.9)	-44.3 (0.6)	-61.4 (4.6)	-44.2 (4.3)
I10	-66.4 (1.1)	-28.1 (0.9)	-48.7 (3.1)	-32.2 (9.7)

	Closed		Semiclosed		Open	
	φ	ψ	φ	ψ	φ	ψ
E11	-91.6 (1.2)	-48.4 (1.3)	-69.0 (11.0)	-27.0 (13.0)	-98.3 (12.6)	-2.5 (3.7)
G12/N12	-112.7 (1.2)	-29.3 (1.4)	-96.0 (13.0)	-8.0 (12.0)	-135.5 (23.7)	32.9(37.9)

	Closed/Semiclosed		Open	
	φ	ψ	φ	ψ
G13	44.3 (1.0)	-145.6 (1.2)	27.3 (117.5)	5.3 (14.2)
W14	-50.5 (0.4)	-61.4 (1.1)	-39.9 (3.3)	-41.6 (3.5)
T15/E15	-49.3 (0.9)	-33.1 (1.1)	-52.6 (3.8)	-33.2 (4.2)
G16	-69.8 (1.5)	-37.1 (0.6)	-70.2 (5.9)	-18.4 (8.5)
M17	-59.4 (1.2)	-46.7 (2.3)	-97.7 (10.8)	-10.7 (3.6)
I18	-62.4 (0.9)	-50.5 (1.2)	-70.7 (5.5)	-45.6 (8.9)
D19	-53.9 (2.7)	-43.5 (1.7)	-35.9 (44.7)	95.5 (89.7)
G20	-68.1 (2.2)	-34.4 (1.1)	63.1 (64.1)	-41.6 (58.7)
W21	-62.8 (1.3)	-48.8 (2.5)		
Y22	-75.8 (2.7)	-31.3 (2.8)		
G23	47.0 (51.6)	30.1 (86.0)		

15. Hydrophobic Surface Area. The POPS program with 1.4 Å probe radius is used to calculate

this area for the closed and semiclosed structures.[17] The hydrophobic surface area of a particular

peptide is then calculated as a weighted average using the best-fit f_c and $f_s = 1 - f_c$ of the

closed/semiclosed model.

Table S8: Hydrophobic surface areas.

Sample	Area (Å^2)
HA3fp20, pH 7.0	1150
HA3fp20, pH 5.0	1169
HA1fp23, pH 7.0	1298
HA1fp23, pH 5.0	1316

References

(1)   Chang, C. D.; Waki, M.; Ahmad, M.; Meienhofer, J.; Lundell, E. O.; Haug, J. D. *Int. J. Peptide Protein Research* **1980**, *15*, 59.
(2)   Lapatsanis, L.; Milias, G.; Froussios, K.; Kolovos, M. *Synthesis* **1983**, *8*, 671.
(3)   Worman, H. J.; Brasitus, T. A.; Dudeja, P. K.; Fozzard, H. A.; Field, M. *Biochemistry* **1986**, *25*, 1549.
(4)   Struck, D. K.; Hoekstra, D.; Pagano, R. E. *Biochemistry* **1981**, *20*, 4093.
(5)   Gullion, T.; Schaefer, J. *J. Magn. Reson.* **1989**, *81*, 196.
(6)   Zheng, Z.; Yang, R.; Bodner, M. L.; Weliky, D. P. *Biochemistry* **2006**, *45*, 12960.
(7)   Gullion, T.; Baker, D. B.; Conradi, M. S. *J. Magn. Reson.* **1990**, *89*, 479.
(8)   Morcombe, C. R.; Zilm, K. W. *J. Magn. Reson.* **2003**, *162*, 479.
(9)   Zhang, H. Y.; Neal, S.; Wishart, D. S. *J. Biomol. NMR* **2003**, *25*, 173.
(10)   Mueller, K. T. *J. Magn. Reson. Ser. A* **1995**, *113*, 81.
(11)   Sun, Y.; Weliky, D. P. *J. Am. Chem. Soc.* **2009**, *131*, 13228.
(12)   Lorieau, J. L.; Louis, J. M.; Schwieters, C. D.; Bax, A. *Proc. Natl. Acad. Sci. U.S.A.* **2012**, *109*, 19994.
(13)   Han, X.; Bushweller, J. H.; Cafiso, D. S.; Tamm, L. K. *Nature Struct. Biol.* **2001**, *8*, 715.
(14)   Lorieau, J. L.; Louis, J. M.; Bax, A. *Proc. Natl. Acad. Sci. U.S.A.* **2010**, *107*, 11341.
(15)   Krieger, E.; Joo, K.; Lee, J.; Lee, J.; Raman, S.; Thompson, J.; Tyka, M.; Baker, D.; Karplus, K. *Prot. Struct. Funct. Bioinf.* **2009**, *77*, 114.
(16)   Panahi, A.; Feig, M. *J. Phys. Chem. B* **2010**, *114*, 1407.
(17)   Cavallo, L.; Kleinjung, J.; Fraternali, F. *Nucleic Acids Res.* **2003**, *31*, 3364.